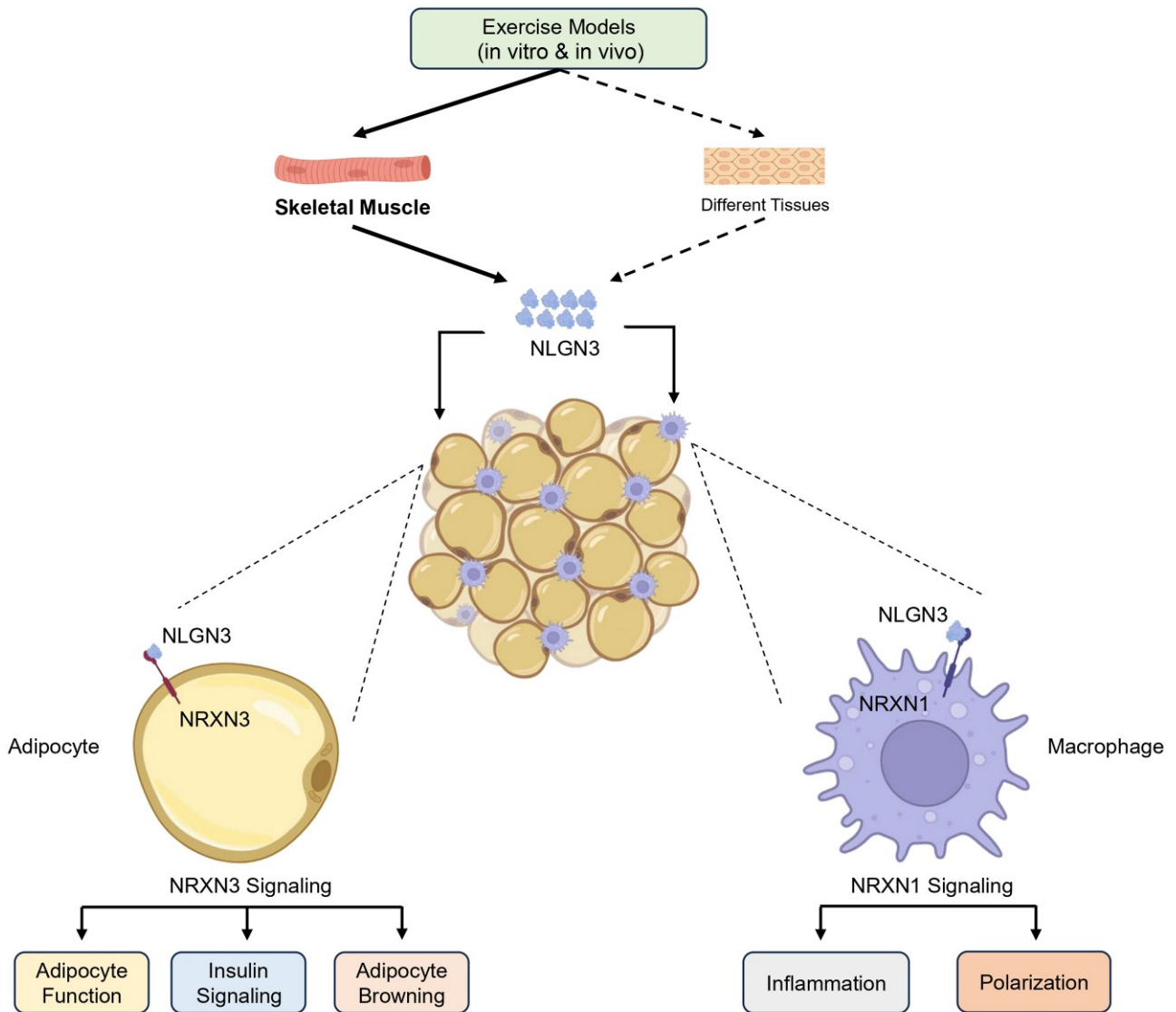


Neuroigin-3: A Novel Exercise-Induced Secreted Factor Enhancing Insulin Sensitivity in Obese Insulin-Resistant Mice

Archana Sinha, Debarun Patra, Subrata Mishra, Ankit Vashisth, Shivam Sharma, Upalabha Dey, Palla Ramprasad, Soumyajit Roy, Aditya Kumar, Kulbhushan Tikoo, Durba Pal, and Suman Dasgupta

Diabetes 2026;75(7):1–16 | <https://doi.org/10.2337/db25-0259>



NLGN, neuroigin; NRXN, neurexin.



Neurotrophin-3: A Novel Exercise-Induced Secreted Factor Enhancing Insulin Sensitivity in Obese Insulin-Resistant Mice

Archana Sinha,¹ Debarun Patra,² Subrata Mishra,¹ Ankit Vashisth,² Shivam Sharma,³ Upalabha Dey,⁴ Palla Ramprasad,² Soumyajit Roy,² Aditya Kumar,⁴ Kulbhushan Tikoo,³ Durba Pal,² and Suman Dasgupta¹

<https://doi.org/10.2337/db25-0259>

The salutary effects of physical exercise in mitigating metabolic disorders, particularly type 2 diabetes, are well recognized. Several studies have demonstrated that endurance training boosts the production of exercise-induced myokines, which are pivotal for interorgan communication enhancing insulin sensitivity. However, several challenges, including an incomplete understanding of underlying molecular mechanisms, hinder their therapeutic application. Here, we have identified a potential exercise-induced mediator, neurotrophin-3 (NLGN3), that enhances insulin sensitivity and abrogates inflammation. Mechanistic studies in white adipocytes revealed that NLGN3 interacts with neurexin-3 (NRXN3) to modulate their function and insulin sensitivity, while in macrophages, NLGN3 engages with NRXN1 to attenuate inflammation and promote an anti-inflammatory phenotype. Administration of NLGN3 in high-fat diet (HFD)-fed mice significantly ameliorated obesity-induced visceral adipose tissue dysfunction and insulin insensitivity; however, these attributes are markedly abolished in NRXN1/3-deficient mice. In addition, elevated serum NLGN3 levels following swimming exercise training correlated with improved metabolic outcomes in HFD-fed obese diabetic mice. These findings suggest that NLGN3 may serve as a key mediator of exercise-induced metabolic benefits and highlight the NLGN3-NRXN1/3 pathway as a promising target for managing obesity-induced insulin resistance.

ARTICLE HIGHLIGHTS

- This study aimed to identify novel exercise-induced myokines and their role in improving insulin sensitivity and reducing inflammation.
- We identified neurotrophin-3 (NLGN3) as an exercise-induced mediator that enhances insulin sensitivity and alleviates inflammation.
- Exercise-induced NLGN3 upregulation or recombinant NLGN3 administration improved metabolic function in high-fat diet-fed mice via neurexin-1 and -3 (NRXN1/3), but these benefits were lost upon NRXN1/3 ablation.
- NLGN3 emerges as a key mediator of exercise-driven metabolic benefits and a promising therapeutic target for obesity-associated insulin resistance.

Obesity-associated metabolic disorders, including type 2 diabetes, represent major global health challenges (1,2). The rising prevalence of obesity-induced type 2 diabetes has prompted extensive research into the molecular mechanisms underlying metabolic dysfunctions, with a particular emphasis on skeletal muscle as an endocrine organ regulating systemic metabolism (3–5). In this context, physical activity is widely recognized as a main intervention for

¹Metabolic Disease Biology Laboratory, Department of Molecular Biology and Biotechnology, Tezpur University, Tezpur, Assam, India

²Department for Biomedical Engineering, Indian Institute of Technology Ropar, Rupnagar, Punjab, India

³Department of Pharmacology and Toxicology, National Institute of Pharmaceutical Education and Research, S.A.S. Nagar, Punjab, India

⁴Genomics and Bioinformatics Laboratory, Department of Molecular Biology and Biotechnology, Tezpur University, Tezpur, Assam, India

Corresponding authors: Suman Dasgupta, suman@tezu.ernet.in or suman.dsut@gmail.com, and Durba Pal, durba.pal@iitrpr.ac.in

Received 19 March 2025 and accepted 8 April 2026

This article contains supplementary material online at <https://doi.org/10.2337/figshare.31972887>.

A.S., D.Pat., S.M., and A.V. contributed equally to this work.

© 2026 by the American Diabetes Association. Readers may use this work for educational, noncommercial purposes if properly cited and unaltered. This publication and its contents may not be reproduced, distributed, or used for text or data mining, machine learning, or other similar technologies without prior written permission. More information is available at <https://diabetesjournals.org/journals/pages/license>.

remediating metabolic health and counteracting metabolic disorders (4–6). A critical component of these benefits is the secretion of different bioactive molecules, collectively called myokines, from contracting skeletal muscle (4–9). Over the past decade, several myokines, including interleukin-6 (IL-6), irisin/fibronectin type III domain containing 5 (FND5), fibroblast growth factor 21 (FGF21), and meteorin-like protein (METRNL), have been identified as key mediators of exercise-induced metabolic improvements (3,8–12); however, the full repertoire of exercise-induced myokines and their specific roles remain incompletely understood.

Neuroigin-3 (NLGN3) is a postsynaptic cell adhesion molecule primarily recognized for its role in synaptic function and neurodevelopment (13–15). NLGN3 interacts with presynaptic neuroligins (NRXN1, NRXN2, and NRXN3) (16), activating Ca^{2+} /calmodulin-dependent Ser/Thr kinase (17), which regulates synaptic structure and function and is essential for neural circuit formation and plasticity (18–20). Emerging evidence has indicated that synaptic proteins and neuronal signaling may also influence metabolic regulation (21,22). However, while the neurobiological roles of NLGN3 and NRXNs are well studied, the contribution of exercise-induced, peripherally derived NLGN3 and the metabolic actions of the NLGN3-NRXN axis in white adipose tissue (WAT) and insulin sensitivity remain unexplored.

Here, we identify NLGN3 as an exercise-induced mediator that enhances adipocyte function, suppresses macrophage inflammation, and improves insulin sensitivity in obese mice, primarily through NRXN1/3 signaling. These findings reveal an unexpected role for NLGN3 in metabolic regulation and highlight its potential as a therapeutic target for obesity-associated insulin resistance.

RESEARCH DESIGN AND METHODS

Reagents and Antibodies

All tissue culture materials were purchased from Life Technologies/Gibco (Grand Island, NY) and Nunc (Corning, NY). Essential resources used are listed in Supplementary Table 1. Gene-specific primers (Supplementary Table 2) were procured from Integrated DNA Technologies, India, and other chemicals from Sigma-Aldrich, St. Louis, MO.

Cell Culture and Treatments

The L6/C2C12 myoblast, RAW264.7 macrophage, and HEK293 embryonic kidney cells were cultured in DMEM containing 1% penicillin-streptomycin with 10% bovine calf serum or FBS, in a 5% CO_2 environment at 37°C (23,24). L6 and C2C12 myoblasts were serum starved (2% FBS) for 7 days to generate myotubes. 3T3-L1 preadipocytes were differentiated into adipocytes over 7 days using insulin (1 $\mu\text{g}/\text{mL}$), 3-isobutyl-1-methylxanthine (0.5 mmol/L), and dexamethasone (1 $\mu\text{mol}/\text{L}$). L6 myotubes were treated with or without caffeine (CAF) (10 mmol/L), forskolin (FSK) (4 $\mu\text{mol}/\text{L}$), or ionomycin (IMY) (0.5 $\mu\text{mol}/\text{L}$) for 8 h, and conditioned media (CM) were collected, desalted using a

PD-10 column, and applied to cell incubations or subjected to liquid chromatography–tandem mass spectrometry (LC-MS/MS). Untransfected or NRXN1-antisense oligonucleotide (ASO)/NRXN2-ASO/NRXN3-ASO-transfected cells were treated with insulin (100 nmol/L) plus palmitate (0.75 mmol/L) or lipopolysaccharide (LPS) (100 ng/mL) in the presence or absence of CM or wild-type (WT)-NLGN3 or mutant (Mut) 1/2-NLGN3 for 5 h before downstream analyses.

LC-MS/MS Analysis

CM samples (CM-control [CM-Con], CM-CAF, CM-FSK, CM-IMY) were lyophilized, trypsin digested (50:1 overnight at 37°C), and centrifuged, and 10- μL aliquots were analyzed on a C18-ultra-performance liquid chromatography column coupled to a Waters Synapt G2 Q-TOF. Data were converted to mzML using MSConvert and mapped against the *Rattus norvegicus* (taxonomy ID 10116) FASTA entries using Morpheus, and identified peptides were aligned to UniProtKB sequences. Proteomic profiles of treated CM were compared with CM-Con; fold changes were calculated and \log_2 -transformed, and proteins unique to treated samples were identified. Among 103 common proteins, relative abundance was z scaled and visualized by heat map. Gene ontology enrichment was performed using gprofiler2 in R. Secretory proteins were predicted using SignalP 5.0, identifying 31 candidates, which were clustered using Pheatmap in R and ranked by mean abundance across treatments. The top five candidates were selected for further validation. Data are available via ProteomeXchange (PXD061199).

Mouse Models and Treatment

WT C57BL/6J male mice (5–6 weeks, 20–24 g) were housed under controlled conditions (12-h light/dark cycle, 23 \pm 2°C, 55 \pm 5% humidity) with free access to food and water. The diet-induced obese insulin-resistant mouse model was established by feeding a high-fat diet (HFD) (60% kcal from fat) for 14 weeks, while controls received a standard diet (10% kcal from fat). Blood glucose was regularly monitored using an Accu-Chek Glucometer (Roche).

Standard diet-fed mice received Invivofectamine-encapsulated control-ASO-locked nucleic acid (LNA) or NLGN3-ASO-LNA (2.5 mg/kg body weight via tail vein) three times over 14 days. Beginning 48 h after each ASO-LNA administration, mice underwent a 14-day swimming regimen, progressively increasing from three 10-min sessions (first 3 days) to three 30-min sessions (next 11 days) per day (25). Similarly, HFD-fed mice were given control-ASO-LNA, NRXN1-ASO-LNA, or NRXN3-ASO-LNA three times over 12 or 14 days followed by PBS or NLGN3 (2 $\mu\text{g}/\text{mouse}$) delivery three times after every 48 h of ASO-LNA administration for 12 days or underwent a 14-day swimming regimen following the above-mentioned protocol. On day 12 or 14, mice were used for various analyses. Glucose tolerance tests (GTTs) were performed after oral gavages of glucose (1g/kg body weight) and insulin tolerance tests (ITTs) after insulin injection (1 IU/kg body weight). Plasma insulin was measured by

ELISA and insulin resistance evaluated by HOMA of insulin resistance (HOMA-IR) using the following equation: fasting insulin (mU/L) \times fasting glucose (mmol/L) / 22.5 (26). Visceral adipose tissue (VAT), liver, and skeletal muscle were collected for hematoxylin-eosin (H-E), oil-red O, and immunostaining or for gene and protein expression analyses. Separately, C57BL/6 mice were also subjected to controlled fasting-refeeding paradigms, involving 12 h or 24 h of fasting followed by ad libitum refeeding for 6 h. Serum and tissue samples were collected to measure circulating NLGN3 levels. In parallel, another cohort underwent an acute 30-min swimming exercise in a temperature-controlled tank without prior training, and blood samples were collected at baseline and 60–240 min after exercise. Serum NLGN3 was quantified by ELISA. All animal procedures followed institutional guidelines and were approved by the animal ethics committee (IAEC/22/37-M).

Reanalysis of Transcriptomic Data Sets

Gene Expression Omnibus data set GSE108643 was reanalyzed for differential gene expression in R (version 4.3.1) using DESeq2, and volcano plots were generated using ggplot2 to compare pre- and postexercise conditions. Single-cell RNA sequencing (RNA-seq) data sets (GSE176171, GSE17617, GSE136103, E-MTAB-13874) were reanalyzed to assess the expression levels and the proportion of cells expressing NRXN1/2/3 in adipocytes and macrophages from human adipose tissue. In addition, the Gene Expression Profiles of RNA-Seq–Based Exercise Responses (GEPREP) database for healthy participants (27) were included in the analysis, including inactive/sedentary control ($n = 491$), aerobic exercise ($n = 163$), and resistance exercise ($n = 222$). Gene expression was analyzed as $\log_2(\text{transcripts per million} + 1)$ to stabilize variance while preserving biological interpretability.

Glucose Uptake Assay

Glucose uptake assay was performed using a glucose uptake cell-based assay kit according to the manufacturer's instructions, as previously described (28,29). Briefly, cells (1×10^4 /well) were serum starved overnight in Krebs' ringer bicarbonate buffer (2% FBS) and treated with palmitate (0.75 mmol/L, 6 h), insulin (100 nmol/L, 30 min), and 2-NBDG (100 $\mu\text{g}/\text{mL}$, 10 min). After lysis, fluorescence was measured using a Varioskan-LUX Multimode Reader (Thermo Fisher Scientific, Vantaa, Finland).

Lipolysis Assay

Control and treated adipocytes (1×10^5 /well) were subjected to lipolysis assay by measuring free glycerol release using a glycerol cell-based assay kit according to the manufacturer's instructions, as previously described (29).

Site-Directed Mutagenesis

WT-NLGN3 (Plasmid 59318; Addgene) was used to generate deletion mutant ($\Delta 560$ –564) using a QuikChange Lightning

Multi Site-Directed Mutagenesis Kit. Primers were designed by the QuikChange Primer Design Program and are listed in Supplementary Table 2.

Immunoblotting

Immunoblot analysis was performed following our previously described method (29,30). Briefly, protein concentration of cell or tissue lysates was determined using a Pierce BCA Protein Assay Kit. Lysate (50 μg protein) was subjected to 10% SDS-PAGE and transferred onto polyvinylidene difluoride membranes using the Bio-Rad Wet/Tank Blotting System. Membranes were blocked with 5% BSA, probed with primary antibodies (1:500 or 1:1,000), washed with Tris-buffered saline (TBS) with Tween 20 (TBST), incubated with peroxidase-conjugated secondary antibodies (1:10,000), then washed twice with TBST and once with TBS. Protein bands were visualized with Clarity Western ECL Substrate using the ChemiDoc XRS+ System (Bio-Rad Laboratories, Hercules, CA) and Image Lab Software.

Semiquantitative and Real-Time Quantitative PCR

Total RNA was extracted from VAT and adipocytes using the RNeasy Lipid Tissue Mini Kit and from liver, skeletal muscle, and macrophages using TRI Reagent. RNA was treated with DNase-I and reverse transcribed using iScript Reverse Transcription Supermix. Semiquantitative RT-PCR was performed with 2 \times PCR Master Mix on a Bio-Rad C1000 Thermal Cycler using gene-specific primers and β -actin as the loading control. Real-time quantitative PCR (qPCR) was conducted on an ABI 7500 system with iTAQ Universal SYBR Green Supermix and gene-specific primers, followed by melting curve analysis. Expression fold changes were calculated using $2^{\Delta\Delta\text{Ct}}$ and normalized to β -actin.

RNA Interference Study

Cells (3×10^6 /well) were transfected with control-ASO or NRXN1/2/3-ASO using Lipofectamine RNAiMAX Transfection Reagent according to the manufacturer's instructions, and knockdown efficiency was analyzed by RT-PCR.

ELISA

Serum NLGN3 and plasma insulin levels were measured using mouse NLGN3 and insulin ELISA kits according to the manufacturer's instructions.

Cycloheximide Chase Assay

C2C12 myotubes were treated with exercise signaling inducers (CAF, FSK, and IMY) for 8 h, followed by cycloheximide (50 $\mu\text{g}/\text{mL}$). NLGN3 levels in the CM were analyzed at various time points by Western blotting.

Immunofluorescence Staining

Immunofluorescence staining of VAT was performed following a method described earlier (31). Briefly, VAT samples were fixed in 10% neutral buffer formalin, cryosectioned (10 μm),

and immunostained with specific primary antibodies followed by DAPI counterstaining. Images were captured and analyzed using a DMi8 microscope (Leica, Wetzlar, Germany) using LAS X software.

H-E Staining

VAT, liver, and skeletal muscle cryosections were stained with H-E, mounted with dibutylphthalate polystyrene xylene solution, and imaged as described earlier (31). Adipocyte size and number were quantified using ImageJ with Adipocyte Tools plugin.

Statistical Analyses

Data are presented as mean \pm SD. Statistical significance was determined using the Student *t* test for two-group comparisons and two-way ANOVA for multiple groups, with *P* < 0.05 considered significant. Data analyses were performed using GraphPad Prism (version 9.0). Methods pertinent to the supplementary figures are provided in the Supplementary Material.

Data and Resource Availability

The MS proteomics have been deposited in the ProteomeXchange Consortium via the PRIDE repository (ID: PXD061199). Additional data sets are available from the corresponding authors upon request. All resources used in this study are detailed in the Supplementary Tables 1–3.

RESULTS

Identification of NLGN3 as a Putative Exercise-Induced Mediator

Skeletal muscle contractions during exercise activated multiple signaling pathways, including AMPK and peroxisome proliferator-activated receptor- γ coactivator-1 α (PGC-1 α), thereby increasing glucose uptake to meet elevated energy demands (10,32). We modeled exercise-induced signaling in skeletal muscle cells in vitro using exercise mimetics (CAF, FSK, and IMY) commonly used to activate exercise-associated pathways regulating myokine expression and release (33,34). Dose-response studies revealed that these exercise mimetics significantly increased cellular 2-NBDG uptake (Supplementary Fig. 1A), which coincided with enhanced PGC-1 α expression and AMPK activation (Supplementary Fig. 1B), without detectable cytotoxicity in L6 myotubes (Supplementary Fig. 1C). To explore exercise-induced myokines in reversing insulin resistance, we collected CM from L6 myotubes treated with or without CAF, FSK, or IMY (Supplementary Fig. 1D) and subsequently incubated them with 3T3-L1 adipocytes. CM-CAF, CM-FSK, and CM-IMY significantly alleviated palmitate-induced impairment of insulin-stimulated 2-NBDG uptake in 3T3-L1 adipocytes compared with CM-Con (Fig. 1A), excluding the contribution of exercise-unrelated factors in the CM to the observed effects. We further tested these CM on palmitate-induced suppression of basal glucose uptake and insulin-stimulated lipolysis and found that while CM-CAF and CM-IMY restored glucose uptake

(Supplementary Fig. 2A), CM-CAF and CM-FSK enhanced glycerol release (Supplementary Fig. 2B). Further analysis elucidated that these CM effectively promoted insulin responsiveness and counteracted palmitate-induced inhibition of insulin signaling molecule phosphorylation (Fig. 1B and C), suggesting that skeletal muscle cell-derived mediators in CM-IMY, CM-CAF, and CM-FSK contributed to improved insulin sensitivity in skeletal muscle and adipocytes.

Obesity is marked by adipose tissue dysbiosis with elevated LPS levels, accompanied by increased macrophage infiltration and a higher prevalence of proinflammatory M1 over anti-inflammatory M2 polarization, thereby promoting chronic inflammation and insulin resistance (35–38). We therefore examined the efficacy of these CM to mitigate inflammation in macrophages. CM-CAF and CM-IMY markedly suppressed LPS-stimulated expression of proinflammatory cytokines while restoring anti-inflammatory cytokines in RAW264.7 macrophages (Supplementary Fig. 2C). Additionally, these CM substantially inhibited LPS-induced activation of nuclear factor- κ B (NF- κ B) p65, extracellular signal-regulated kinase (ERK), and p38 MAPK compared with CM-Con (Fig. 1D and Supplementary Fig. 2D). In addition, these CM reduced the proinflammatory phenotype in LPS-treated macrophages while promoting an anti-inflammatory state, as evidenced by reduced CD68 and elevated CD163 levels (Supplementary Fig. 2E). Furthermore, these CM significantly suppressed LPS-induced κ B-luciferase (luc) activity and phagocytosis in macrophages (Supplementary Fig. 2F and G). Together, these findings suggest that candidate mediators present in CM-CAF, CM-FSK, and CM-IMY could modulate adipocytes and macrophages in WAT, thereby potentially enhancing insulin sensitivity and reducing inflammation.

To identify the putative exercise-induced mediators, CM-Con, CM-CAF, CM-FSK, and CM-IMY were subjected to LC-MS/MS analysis (Supplementary Fig. 2H and I). Differential profiling revealed 465, 429, and 417 unique proteins in CM-CAF, CM-FSK, and CM-IMY, respectively, with 103 proteins common to all three conditions but absent in CM-Con (Fig. 1E). Heat map and gene ontology analysis of these 103 proteins showed variations in abundance across treatments and enrichment in diverse functions (Supplementary Fig. 2J and K). Among these 103 proteins, 31 have a signal sequence as predicted by the Signal-IP algorithm (39), suggesting their secretion. These proteins were ranked by their mean abundance (Fig. 1F), with gene ontology analysis linking them to glutamate receptor signaling, ion channel activity, and calcium-mediated signaling (Supplementary Fig. 2L). Among the identified secretory proteins, NLGN3, NMDE2, GRM3, LRP4, and A2MG emerged as top candidates (Supplementary Fig. 2M). Gene expression analysis supported the proteomic findings, showing a colossal increase of NLGN3 gene expression in L6 myotubes treated with the exercise mimetics (Supplementary Fig. 2N). To assess exercise-induced transcriptional changes in human skeletal muscle, we reanalyzed the Gene Expression Omnibus

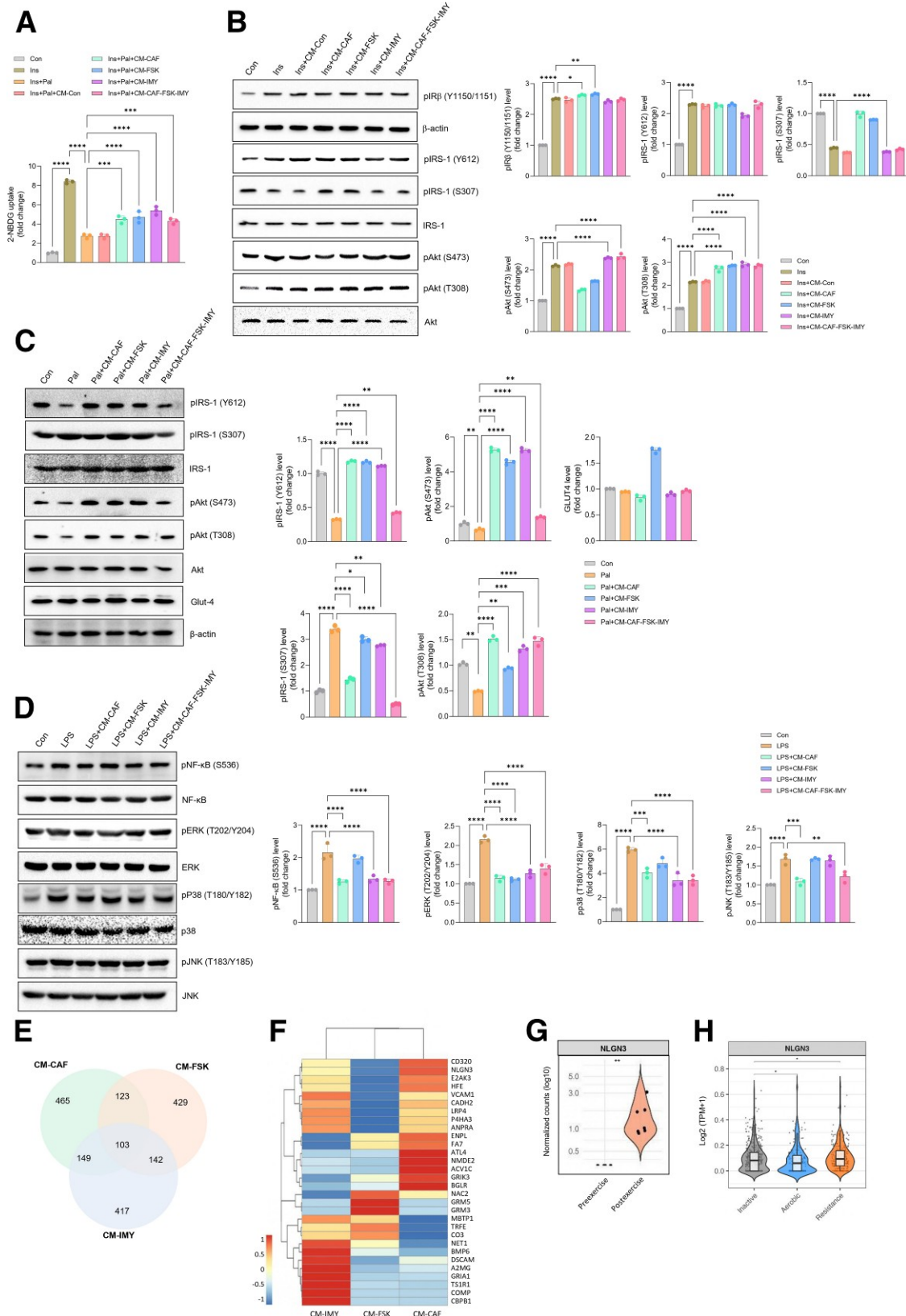


Figure 1—Identification of NLGN3 as a putative exercise-induced mediator. **A**: Determination of insulin (Ins)-stimulated 2-NBDG uptake by 3T3-L1 adipocytes exposed to CM from L6 myotubes treated without (CM-Con) or with CAF (10 mmol/L), FSK (4 μmol/L), IMY (0.5 μmol/L), or a combination of all (CM-CAF-FSK-IMY) in the presence or absence of Ins (100 nmol/L) with or without palmitate (Pal) (0.75 mmol/L) for 6 h. **B**: Western blot analysis depicting the abundance of pIRβ (Y1150/1151), pIRS-1 (Y612), pIRS-1 (S307), pAkt (T308), and pAkt (S473) proteins in 3T3-L1 adipocytes following exposure to CM-Con, CM-CAF, CM-FSK, CM-IMY, or CM-CAF-FSK-IMY in the

data set GSE108643 from lean individuals before and after acute aerobic exercise. DESeq2 analysis revealed a significant postexercise upregulation of NLGN3, ERFE, and VEGF-A (Fig. 1G and Supplementary Fig. 2O). Additionally, we explored the human GEPREP database, a comprehensive atlas of RNA-seq data sets of exercise-responsive gene expression, and found a significant induction of NLGN3 expression in skeletal muscle following exercise (Fig. 1H), alongside established myokines such as IL-6 and myostatin (Supplementary Fig. 2P), further supporting NLGN3 as an exercise-responsive, muscle-derived factor. Moreover, NLGN3 showed high sequence similarity across various organisms, including humans (Supplementary Fig. 2Q). These observations prompted us to investigate NLGN3's potential in metabolic function.

NLGN3 Prevents Adipocyte Dysfunction and Macrophage Inflammation

NLGN3 is traditionally known for roles in synapse formation and signaling (13,14). However, our findings demonstrate that NLGN3 is secreted in response to exercise signaling in L6 myotubes, identifying it as a potential exercise-induced mediator. To assess the metabolic function of NLGN3, we examined its effect on insulin sensitivity. WT-NLGN3 significantly restored insulin-stimulated 2-NBDG uptake impaired by palmitate and enhanced insulin action in 3T3-L1 adipocytes and C2C12 myotubes, whereas Mut1-NLGN3 (R541C) and Mut2-NLGN3 (Δ 560–564) failed to do so (Fig. 2A and B and Supplementary Fig. 3A–D). NLGN3 exerts its effects through binding to its cognate receptors NRXN1, NRXN2, and NRXN3 (18–20). To identify the specific NRXN isoform that mediates NLGN3's effect in white adipocytes, we introduced ASOs against NRXN1/2/3 in 3T3-L1 adipocytes. Results yielded three important findings: 1) mouse white adipocytes expressed NRXN3, with no detectable NRXN1/2; 2) NRXN3-ASO significantly downregulated NRXN3 expression; and 3) NRXN1/2-ASOs had no significant impact on NRXN3 expression, confirming target specificity (Supplementary Fig. 3E). Loss-of-function studies in adipocytes demonstrated that NRXN3 silencing, but not NRXN1/2, abolished the ability of WT-NLGN3 to reverse palmitate-induced inhibition of 2-NBDG uptake (Fig. 2C). WT-NLGN3 strikingly rescued palmitate-induced inhibition

of insulin signaling molecule activation in 3T3-L1 adipocytes, whereas Mut1/2-NLGN3 showed no such effect. Notably, NRXN3 knockdown blocked WT-NLGN3-induced phosphorylation of these signaling molecules (Fig. 2D), establishing NRXN3 as the functional receptor mediating NLGN3 effects in mouse adipocytes.

Adipocyte function is primarily regulated by homeostatic balance of adipogenesis, lipogenesis, and lipolysis (40–42). WT-NLGN3, but not Mut1/2-NLGN3, significantly inhibited adipogenesis in 3T3-L1 cells (Supplementary Fig. 3F). While WT-NLGN3 incubation increased both triglyceride and glycerol release from adipocytes, Mut1/2-NLGN3 treatment and NRXN1/3 silencing selectively reduced glycerol release without significantly diminishing extracellular triglyceride levels (Supplementary Fig. 3G and H). Since glycerol release directly reflects triglyceride hydrolysis, these data indicate that NRXN1/3 signaling is specifically required for lipolysis. In contrast, extracellular triglyceride levels may reflect additional receptor-independent lipid handling processes, explaining their persistence despite NLGN3 mutation or NRXN1/3 ablation. These results highlight the role of the NLGN3-NRXN3 axis in driving spontaneous lipolysis.

Next, we sought to investigate the efficacy of WT-NLGN3 and its receptors in the reversal of LPS-induced inflammation and stress signaling in RAW264.7 macrophages. WT-NLGN3 markedly suppressed LPS-induced activation of inflammatory and stress markers, whereas Mut1/2-NLGN3 failed to do so (Fig. 2E). Importantly, introducing NRXN1-ASO, but not NRXN2/3-ASOs, in mouse macrophages (Supplementary Fig. 3I) significantly impaired WT-NLGN3's ability to suppress the LPS-induced activation of inflammatory and stress signaling markers (Fig. 2F). Intriguingly, similar to mouse adipocytes, a differential expression pattern for NRXNs was showcased in mouse macrophages, with NRXN1 being abundant in macrophages but not NRXN3 (Supplementary Fig. 3E and J). Consistently, WT-NLGN3 inhibited κ B-luc, AP1-luc, and IRF3-luc transactivation, an effect lost upon NRXN1 silencing (Supplementary Fig. 3J). Interestingly, mouse skeletal muscle cells expressed both isoforms (Supplementary Fig. 3K), with pronounced effects of NLGN3 on glucose uptake in C2C12 myotubes (Supplementary Fig. 3C). These findings suggest a possible link of NLGN3-NRXN1 pathway stimulation

presence or absence of Ins (100 nmol/L) for 6 h. Total IRS-1, Akt, and β -actin served as loading controls. C: Western blot analysis depicting the abundance of pIRS-1 (Y612), pIRS-1 (S307), pAkt (T308), pAkt (S473), and Glut-4 proteins in 3T3-L1 adipocytes following exposure to CM-CAF, CM-FSK, CM-IMY, or CM-CAF-FSK-IMY in the presence or absence of Pal for 6 h. Total IRS-1, Akt1/2/3, and β -actin served as loading controls. D: Western blot analysis showing the abundance of pNF- κ B (S536), pERK (T202/Y204), pp38 (T180/Y182), and pJNK (T183/Y185) in RAW264.7 macrophages treated with CM-CAF, CM-FSK, CM-IMY, or CM-CAF-FSK-IMY in the presence or absence of LPS for 6 h. Total NF- κ B, ERK, p38, and JNK served as loading controls. E: Venn diagram from the proteomic analysis illustrating the number of uniquely expressed proteins in CM-CAF, CM-FSK, and CM-IMY of L6 myotubes. F: Heat map analysis of 31 shared proteins commonly available in the CM-CAF, CM-FSK, and CM-IMY. G: Violin plots showing the normalized counts (\log_{10}) of NLGN3 gene expression levels in lean individuals before and after exercise. H: Violin plots depicting the distribution of NLGN3 gene expression levels [\log_2 (transcripts per million [TPM] + 1)] in skeletal muscle of healthy human participants from the GEPREP database, stratified by exercise status: inactive (sedentary control), aerobic exercise, and resistance training. Embedded box plots indicate the median and interquartile range, with individual data points represented as jittered dots. Statistical significance was determined using Wilcoxon rank sum tests with Benjamini-Hochberg correction for multiple comparisons. All experiments were performed in triplicate. Data are mean \pm SD of three independent experiments. * P < 0.05, ** P < 0.01, *** P < 0.001, **** P < 0.0001.

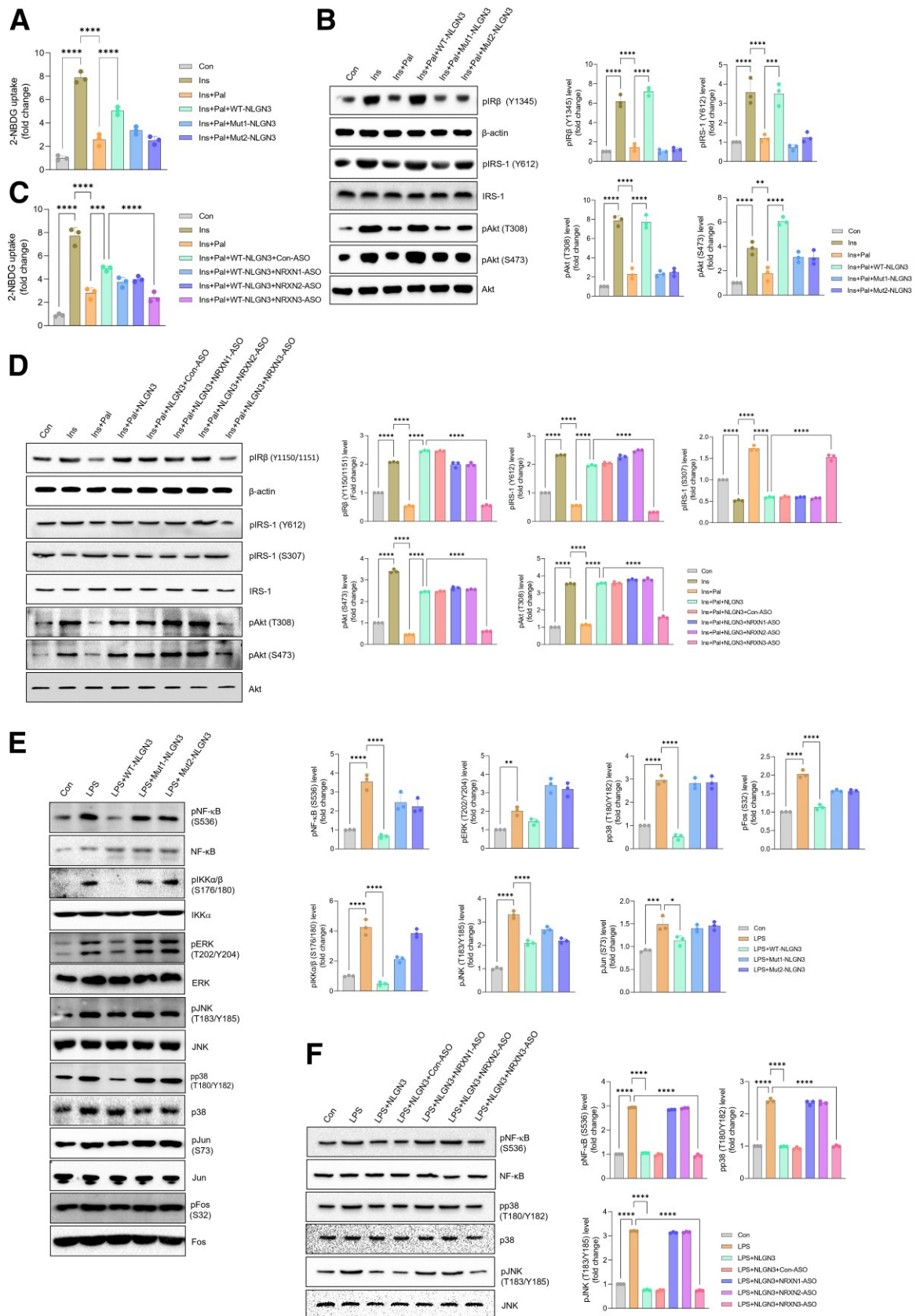


Figure 2—NLGN3 prevents adipocyte dysfunction and macrophage inflammation. **A**: Analysis of insulin (Ins)-stimulated 2-NBDG uptake by 3T3-L1 adipocytes following incubation with WT-NLGN3 or Mut1/2-NLGN3 (10 ng/mL) in the presence or absence of Ins (100 nmol/L) with or without palmitate (Pal) (0.75 mmol/L) for 6 h. **B**: Western blot analysis showing the levels of pIR β (Y1345), pIRS-1 (Y612), and pAkt (T308 and S473) in 3T3-L1 adipocytes treated with WT-NLGN3 or Mut1/2-NLGN3 in the absence or presence of Ins or Ins + Pal for 6 h.

in the attenuation of LPS-induced inflammation and stress signaling in macrophages.

Given the lipid-enrich nature of obese WAT, we delved into NLGN3's role in insulin signaling and inflammation in NRXN3- and NRXN1-silenced adipocytes and macrophages, respectively, under palmitate exposure. NLGN3 restored Glut4 expression suppressed by palmitate, an effect lost in NRXN3-ASO-treated adipocytes (Supplementary Fig. 3L). Since NF- κ B is a master regulator governing cellular inflammation (43), we examined NLGN3's effect on palmitate-induced NF- κ B activation. NLGN3 attenuated palmitate-induced NF- κ B activation (Supplementary Fig. 3M) and shifted polarization toward an anti-inflammatory state as indicated by decreased CD80 and increased CD206 (Supplementary Fig. 3N), which were abolished by NRXN1 silencing (Supplementary Fig. 3M and N). Together, these findings suggest that NLGN3-NRXN3 and NLGN3-NRXN1 signaling are crucial for enhancing adipocyte insulin sensitivity and resolving macrophage inflammation, respectively.

Exercise Induces NLGN3 and Improves Insulin Sensitivity

To evaluate the physiological relevance of NLGN3 as an exercise-induced mediator, C57BL/6 mice fed a standard diet received control-ASO-LNA or NLGN3-ASO-LNA (Supplementary Fig. 4A) and underwent a 14-day swimming exercise training (Fig. 3A). Exercise markedly elevated circulating NLGN3 levels, which were accompanied by improved insulin sensitivity, as evidenced by the oral GTT, intraperitoneal ITT, HOMA-IR, and lowered fasting insulin levels. These beneficial effects were abrogated in the NLGN3-ASO-treated mice (Fig. 3B–D and Supplementary Fig. 4B and C), without changes in body weight (Supplementary Fig. 4D), food intake (Supplementary Fig. 4E), different tissue weights (Supplementary Fig. 4F), and histological features (VAT, liver, and skeletal muscle) (Supplementary Fig. 4G–I). Gene expression analysis of VAT demonstrated that exercise training elevated mRNA levels of browning markers (UCP1, TMEM26, and PRDM16) and shifted the profile from proinflammatory (IL-1 β and inducible nitric oxide synthase [iNOS]) to anti-inflammatory (ARG1 and YM1) markers. However, these exercise-induced adaptations were markedly attenuated by NLGN3-ASO delivery (Fig. 3E). Consistently, the exercise-induced upregulation of browning marker gene expression in brown adipose tissue (BAT) was blunted in mice administered NLGN3-ASO (Fig. 3F). We performed an *in vitro* cycloheximide chase assay that revealed

an intracellular NLGN3 half-life of \sim 16 h (Fig. 3G), indicating relative protein stability once synthesized. While precise *in vivo* half-life determination of a myokine is challenging due to continuous secretion and systemic clearance, time course analysis following a single bout of exercise is commonly used to estimate apparent circulatory persistence (44). Our data from a single bout of swimming exercise revealed a rapid increase in serum NLGN3, peaking at 60 min postexercise and slowly declining thereafter (Fig. 3H). These results indicate that the enhancement of circulating NLGN3 following exercise primarily represents an acute exercise-induced response. We also conducted fasting-refeeding experiments in mice to assess whether NLGN3 levels are regulated by these physiological states. A 12-h fasting period markedly increased serum NLGN3, which reduced substantially after 6 h of refeeding (Fig. 3I). In contrast, tissue-level analyses revealed divergent regulatory patterns: NLGN3 was elevated in skeletal muscle during refeeding and in liver during fasting (Fig. 3J). Notably, exercise signaling inducers markedly increased NLGN3 levels in skeletal muscle cell CM via both active secretion and proteolytic shedding, with shedding being the dominant mechanism (Supplementary Fig. 4J). Together, these findings indicate that NLGN3 is dynamically regulated in a tissue-specific and context-dependent manner, with skeletal muscle functioning as an exercise- and nutrient-responsive source, while the liver displays reciprocal regulation during fasting-refeeding, consistent with a role in metabolic adaptation.

NLGN3 Reverses Obesity-Induced Impairments of Insulin Sensitivity in Mice

To inspect the therapeutic potential of NLGN3, recombinant NLGN3 was administered to HFD-fed obese mice on days 2, 6, and 10. Prior to NLGN3 delivery, these mice received Con-ASO-LNA or NRXN1/3-ASO-LNA on days 0, 4, and 8, followed by sacrifice or experimentation on day 12 (Fig. 4A). NLGN3 delivery notably reduced epididymal fat weight (Fig. 4B and C), body weight (Supplementary Fig. 5A) in line with previous observations (45), VAT hypertrophy, and adipocyte size (Fig. 4D and E) while increasing adipocyte number (Fig. 4F) in HFD mice, but these effects were prevented by NRXN1/3-ASO-LNA administration (Fig. 4A–F). The increase in adipocyte number per unit area reflected higher cell density from reduced adipocyte size and may not have necessarily indicated an absolute rise in total adipocyte count within the depot. Notably, gene expression analysis

Total IRS-1, Akt, and β -actin served as loading controls. C: Assessment of Ins-stimulated 2-NBDG uptake in 3T3-L1 adipocytes transfected with Con-ASO or NRXN1/2/3-ASO and incubated with or without WT-NLGN3 for 6 h. D: Western blot analysis of the levels of pIR β (Y1345), pIRS-1 (Y612 and S307), pAkt (T308 and S473) in 3T3-L1 adipocytes transfected with NRXN-1/2/3-ASO and treated with NLGN3 in the absence or presence of Ins or Ins + Pal for 6 h. Total IRS1, Akt, and β -actin served as loading controls. E: Western blot analysis showing the abundance of pNF- κ B (S536), pIKK α / β (S176/180), pERK (T202/Y204), pJNK (T183/Y185), pp38 (T180/Y182), pJun (S73), and pFos (S32) in RAW264.7 macrophages transfected with WT-NLGN3 or Mut1/2-NLGN3 in the absence or presence of LPS for 6 h. Total NF- κ B, IKK α , ERK, JNK, p38, Jun, and Fos served as loading controls. F: Western blot analysis showing abundance of pNF- κ B (S536), pp38 (T180/Y182), and pJNK (T183/Y185), in RAW264.7 macrophages transfected with NRXN-1/2/3-ASO and treated with NLGN3 in the absence or presence of LPS for 6 h. Total NF- κ B, p38, JNK served as loading controls. All experiments were performed in triplicate. Data are mean \pm SD of three independent experiments. * P < 0.05, ** P < 0.01, *** P < 0.001, **** P < 0.0001.

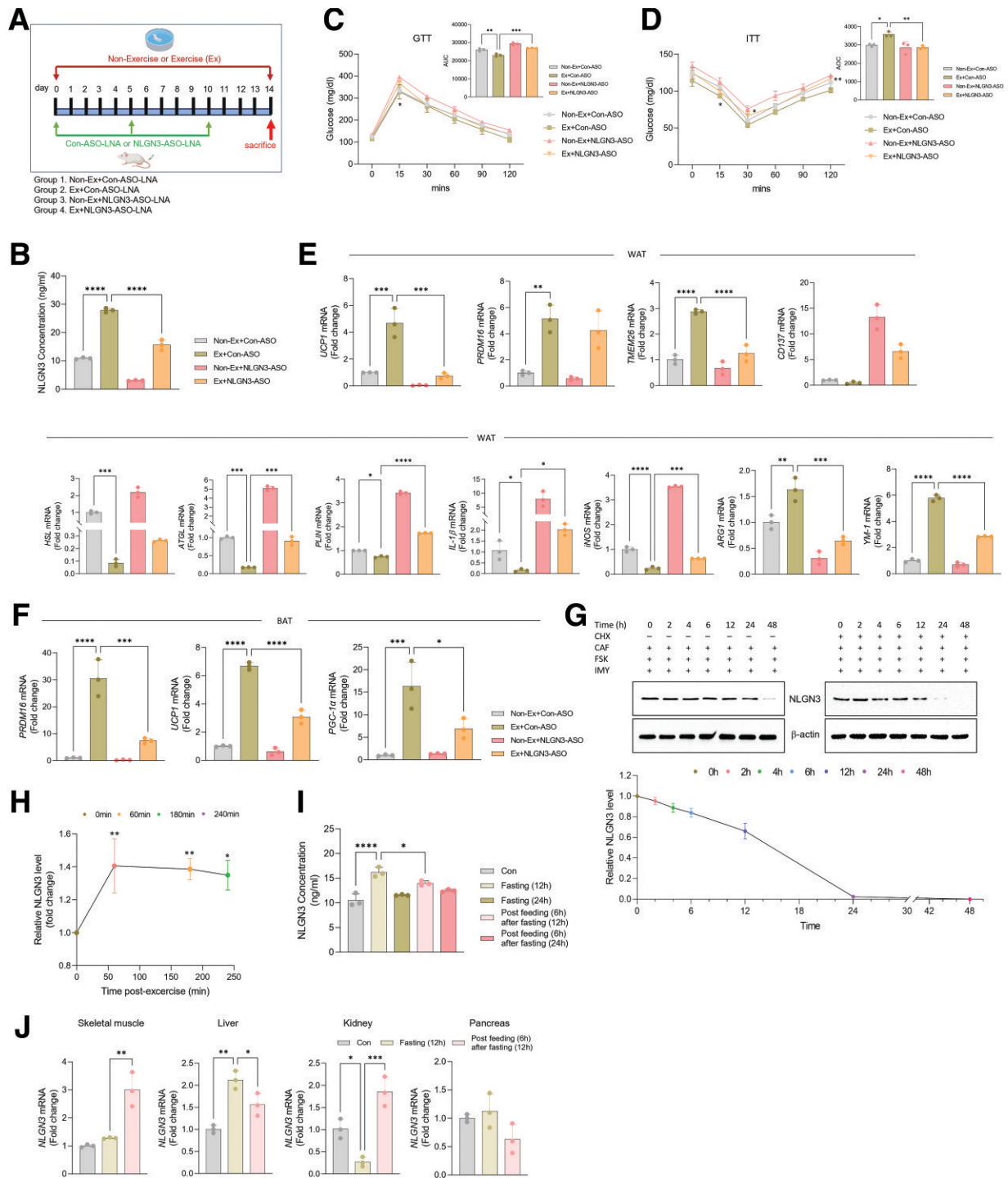


Figure 3—Exercise induces NLGN3 and improves insulin sensitivity. **A**: Schematic illustration of the 14-day swimming exercise regimen combined with the administration schedule of Con-ASO-LNA or NLGN3-ASO-LNA in standard diet-fed mice. **B**: Serum NLGN3 levels were measured by ELISA in the respective treatment groups ($n = 3$). **C** and **D**: Oral GTT with area under curve (AUC) (**C**) and intraperitoneal ITT with area over the curve (AOC) (**D**) were analyzed for the above-mentioned treatment groups ($n = 3$). **E**: RT-qPCR analysis of mRNA expression levels for browning markers (UCP1, TMEM26, PRDM16, and CD137), lipolysis markers (ATGL, HSL, and PLIN), and proinflammatory (iNOS and IL-1 β) and anti-inflammatory (ARG1 and YM1) markers in the WAT from the respective treatment groups ($n = 3$). **F**: RT-qPCR analysis of mRNA expression levels for BAT markers (UCP1, PRDM16, and PGC-1 α) from the respective treatment groups ($n = 3$). **G**: Cycloheximide (CHX) chase assay illustrating NLGN3 protein abundance (top) and its quantification (bottom) in C2C12 myotubes at indicated time points in the presence or absence of CHX treatment (50 μ g/mL). Experiments were performed in triplicate, where each value represents the mean \pm SD of three independent experiments. **H**: Measurement of relative serum NLGN3 levels at indicated time points (0–240 min) following a single 30-min bout of swimming exercise in standard diet-fed C57BL/6 mice ($n = 3$). **I**: Serum NLGN3 concentrations were quantified by ELISA in standard diet-fed C57BL/6 mice following a 12- or 24-h fast and after 6-h of refeeding ($n = 3$). **J**: RT-qPCR analysis of NLGN3 mRNA levels after 12 h of fasting and 6 h of refeeding ($n = 3$). * $P < 0.05$, ** $P < 0.01$, *** $P < 0.001$, **** $P < 0.0001$.

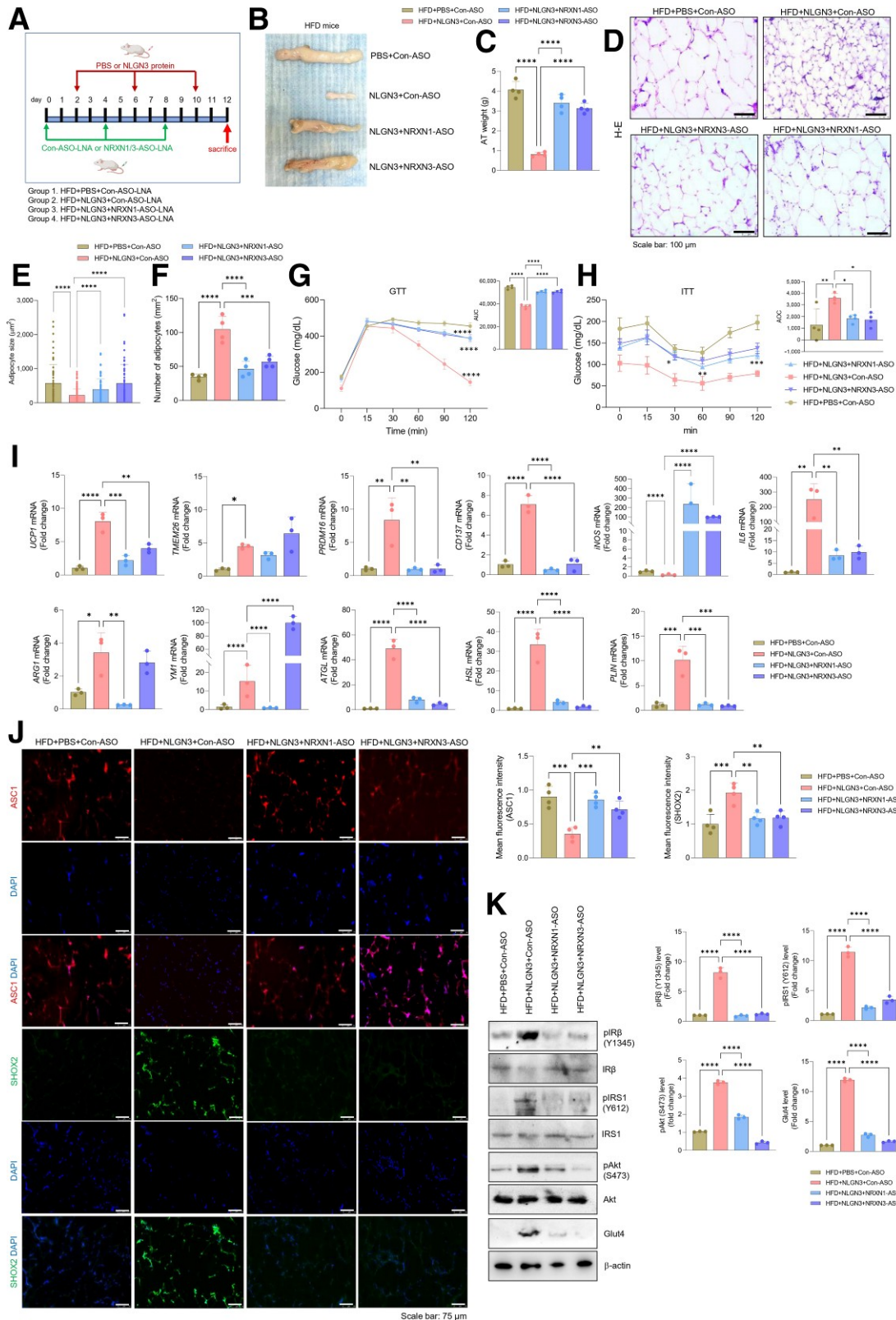


Figure 4—NLGN3 reverses obesity-induced impairments of insulin sensitivity in mice. **A**: Schematic representation of the treatment schedule for Con-ASO-LNA or NRXN1/3-ASO-LNA and NLGN3 or PBS administration in HFD-induced obese mice. **B** and **C**: Representative photographic images of epididymal adipose tissue (**B**) and corresponding weight measurements (**C**) from HFD mice administered Con-ASO-LNA or NRXN1/3-ASO-LNA and treated with either NLGN3 or PBS ($n = 4$). **D–F**: H-E staining images of VAT sections (**D**), along with quantifications of adipocyte size (**E**) and number (**F**) of the above-mentioned mice ($n = 4$). **G** and **H**: Oral GTT with area under the curve (AUC) (**G**) and intra-peritoneal ITT with area over the curve (AOC) (**H**) were analyzed in the same treatment groups ($n = 4$). **I**: RT-qPCR analysis of mRNA expression levels for adipose tissue browning markers (UCP1, TMEM26, PRDM16, and CD137), lipolysis markers (ATGL,

revealed that skeletal muscle expressed both NRXN1 and NRXN3, with NLGN3 administration upregulating their expression, whereas no such induction was detected in the liver (Supplementary Fig. 5B). NLGN3 infusion significantly rescued HFD mice from diet-induced insulin resistance as evident from GTT, ITT, HOMA-IR, and fasting insulin levels; however, these benefits were impaired by NRXN1/3 silencing (Fig. 4G and H and Supplementary Fig. 5C and D). RT-qPCR analysis of VAT revealed increased expression of browning (UCP1, TMEM26, PRDM16, and CD137) and lipolysis (ATGL, HSL, and PLIN) markers, alongside reduced proinflammatory (iNOS and IL-6) and elevated anti-inflammatory (ARG1 and YM1) genes upon NLGN3 treatment (Fig. 4I). These effects were compromised in NRXN1/3-silenced HFD mice (Fig. 4I), consistent with altered NF- κ B activation (Supplementary Fig. 5E). While in vitro data suggested that NRXN3 mediates adipocyte lipolysis and NRXN1 regulates macrophage inflammation, in vivo silencing of either receptor disrupted NLGN3's metabolic benefits, likely reflecting a complex interplay between insulin sensitivity and inflammation in which disruption of one process exacerbates the other in a vicious cycle. Given the robust induction of lipolytic genes in VAT of HFD-fed mice after NLGN3 administration, we next examined ectopic lipid deposition. Oil-red O staining demonstrated reduced hepatic lipid deposition with NLGN3 treatment, which substantially reversed by NRXN1/3-ASO-LNA (Supplementary Fig. 5F and G), although hepatic triglyceride levels remained unchanged (Supplementary Fig. 5H). In skeletal muscle, lipid accumulation was unaffected by NLGN3 delivery or NRXN1/3 silencing (Supplementary Fig. 5I and J). Notably, NLGN3 significantly upregulated β -oxidation marker gene expression in liver and skeletal muscle, while NRXN1/3 silencing attenuated these effects (Supplementary Fig. 5K and L). Thus, NLGN3 appears to limit ectopic lipid deposition and facilitate β -oxidation. NLGN3 administration reduced ASC1 (white adipocyte marker) and induced SHOX2, UCP1, and PGC-1 α (brown/beige adipocyte markers) abundance in the VAT of HFD mice, an effect markedly undermined by NRXN1/3 silencing (Fig. 4J and Supplementary Fig. 5M and N). Additionally, NLGN3 enhanced activation of insulin signaling molecules (IR β , IRS1, and Akt) and upregulated Glut4 in VAT, liver, and skeletal muscle, which were suppressed by NRXN1/3-ASO (Fig. 4K and Supplementary Fig. 5O and P). Taken together, these results show that NLGN3 application alleviates obesity-induced WAT dysfunction while enhancing insulin sensitivity and glucose homeostasis.

Exercise-Induced NLGN3 Prevents Insulin Resistance in Obese Mice

To investigate the contribution of physical exercise on NLGN3 expression and insulin sensitivity, HFD-fed mice underwent a swimming exercise regimen for 14 days (Fig. 5A). Exercise significantly augmented serum NLGN3 levels in HFD-fed mice, an effect suppressed by NRXN1-ASO-LNA but not NRXN3-ASO-LNA (Fig. 5B), suggesting that NRXN1, rather than NRXN3, may play a role in regulating NLGN3 expression/secretion. For translational relevance, we reanalyzed publicly available single-cell RNA-seq data sets from VAT (GSE176171), liver (GSE136103), and skeletal muscle (E-MTAB-13874) to compare NRXN isoform expression patterns and found that NRXN3 was the most abundantly expressed isoform across tissues, while NRXN2 was less prevalent (Supplementary Fig. 6A). To assess whether nutritional status regulates NLGN3 expression, we found that obesity markedly suppressed NLGN3 mRNA levels in both skeletal muscle and liver (Supplementary Fig. 6B), which coincided with decreased serum NLGN3 levels in obese mice (Supplementary Fig. 6C). Exercise considerably reduced VAT hypertrophy, adipocyte size (Fig. 5C and D), body weight (Supplementary Fig. 6D), and epididymal fat mass (Supplementary Fig. 6E) while increasing adipocyte numbers (Fig. 5E) in HFD mice. These attributes were distinctly reversed in HFD mice upon NRXN1/3-ASO-LNA delivery (Fig. 5C–E and Supplementary Fig. 6D and E). Exercise training upregulated NLGN3 gene expression in VAT and skeletal muscle, with a greater effect in skeletal muscle, and lowered liver triglycerides, whereas NRXN1/3-ASO-LNA delivery selectively suppressed NLGN3 expression (Supplementary Fig. 6F and G). The swimming exercise raised serum NLGN3 by \sim 4.5-fold, comparable to the \sim 5.2-fold increase with recombinant NLGN3 administration (Supplementary Fig. 6H), indicating similar systemic NLGN3 levels between exercise and exogenous treatment under our conditions. Additionally, NRXN1/3-ASO-LNA delivery significantly blocked exercise-induced enhancement of insulin sensitivity, as demonstrated by GTT, ITT, HOMA-IR, and insulin levels (Fig. 5F and G and Supplementary Fig. 6I and J). In HFD-fed mice, exercise increased browning marker, shifted from pro- to anti-inflammatory phenotype marker, and upregulated lipolytic marker gene expression in VAT. However, NRXN1/3-ASO-LNA delivery significantly attenuated exercise-induced changes in browning and inflammatory markers but did not affect lipolytic marker gene expression (Fig. 5H). We also noted exercise-induced NF- κ B inhibition, a decrease in white adipocyte markers, and an increase in brown/beige adipocyte markers in VAT, which were impaired by NRXN1/3 silencing (Fig. 5I and Supplementary Fig. 6K–M). Furthermore, NRXN1/

HSL, and PLIN), and proinflammatory (iNOS and IL6), and anti-inflammatory (ARG1 and YM1) markers in the VAT from the same treatment groups ($n = 3$). J: Representative immunofluorescence images (left) and corresponding fluorescence intensity quantification (right) of ASC1 (white adipocyte marker, green), and SHOX2 (beige/brown adipocyte marker, red) in the VAT sections from HFD-fed mice administered Con-ASO or NRXN1/3-ASO and treated with either NLGN3 or PBS ($n = 4$). K: Western blot analysis showing abundances of pIR β (Y1345), pIRS-1 (Y612), pAkt (S473), and Glut-4 in the VAT from the respective treatment groups ($n = 3$). Total IR β , IRS-1, Akt1/2/3, and β -actin served as loading controls. Data are mean \pm SD. * $P < 0.05$, ** $P < 0.01$, *** $P < 0.001$, **** $P < 0.0001$.

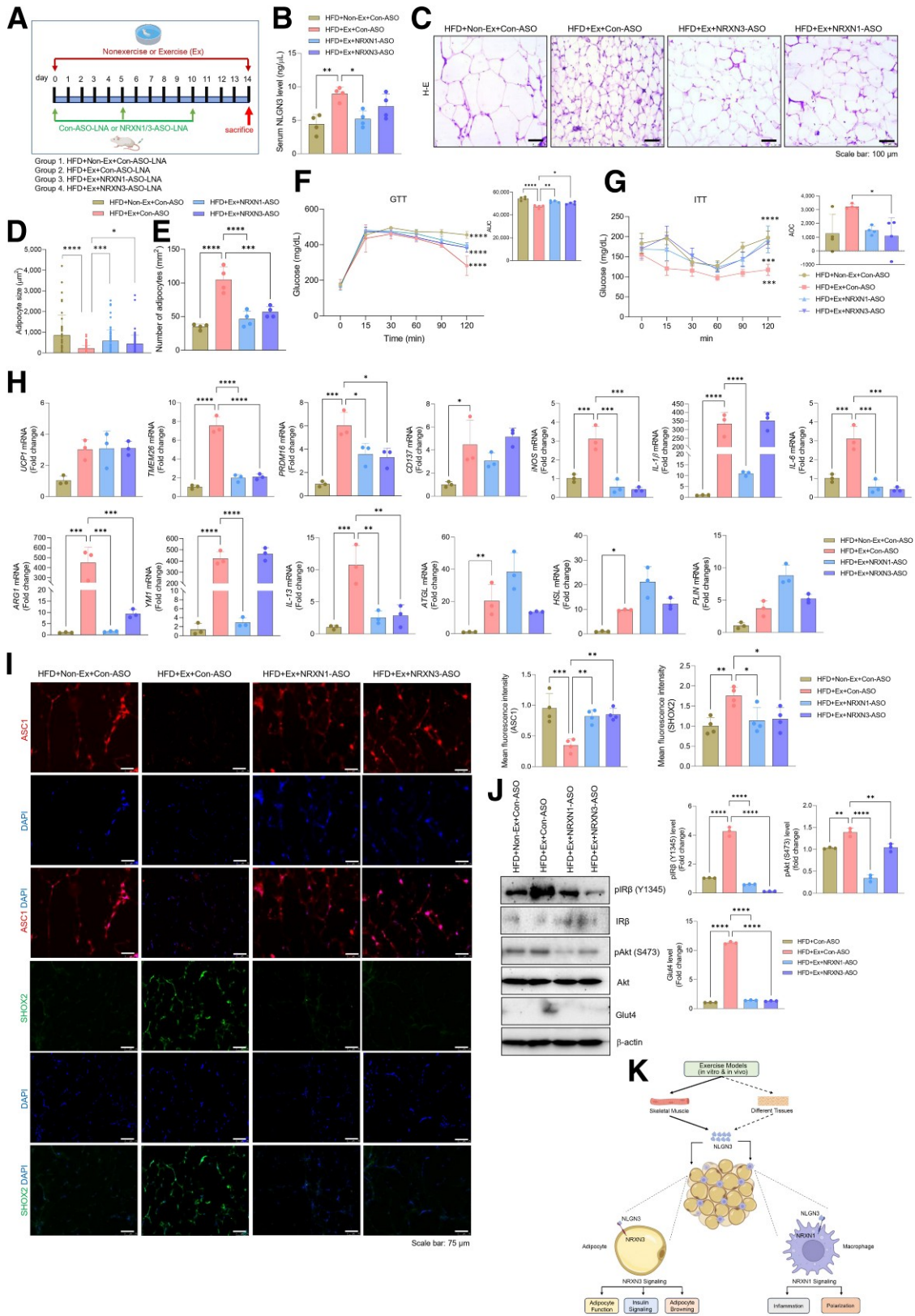


Figure 5—Exercise-induced NLGN3 prevents insulin resistance in obese mice. **A**: Schematic illustration of the 14-day swimming exercise regimen combined with the administration schedule of Con-ASO-LNA or NRXN1/3-ASO-LNA in HFD-fed obese mice. **B**: Serum NLGN3 levels were measured by ELISA in the respective treatment groups ($n = 4$). **C–E**: H-E staining images of WAT sections (**C**), with corresponding quantifications of adipocyte size (**D**) and number (**E**) of HFD mice administered Con-ASO-LNA or NRXN1/3-ASO-LNA with or without exposure to swimming training ($n = 4$). **F–G**: Oral GTT with area under the curve (AUC) (**F**) and intraperitoneal ITT with area over the curve (AOC) (**G**) were analyzed for the above-mentioned treatment groups ($n = 4$). **H**: RT-qPCR analysis of mRNA expression levels for adipose

3-ASO-LNA diminished exercise-induced activation of insulin signaling molecules in VAT, liver, and skeletal muscle of HFD mice (Fig. 5J and Supplementary Fig. 6N and O). Collectively, these findings provide captivating evidence that exercise-induced factor NLGN3 mediates improvements in WAT function and insulin sensitivity in obese insulin-resistant mice. In summary, exercise-induced, skeletal muscle-derived NLGN3 interacts with NRXN1/3 in adipocytes and macrophages, thereby mediating skeletal muscle-adipose tissue cross talk to hoist insulin sensitivity, as illustrated by the schematic diagram in Fig. 5K.

DISCUSSION

Exercise-induced factors have long been recognized for their metabolic benefits. Since IL-6 was identified as the first exercise-induced mediator (46) and the introduction of the myokine concept (8), extensive research has committed to identifying and characterizing these molecules to develop strategies for combating metabolic diseases. In this context, the myokinome has garnered significant attention, with factors such as irisin/FNDC5, FGF21, and METRN standing out among others (3,8–12). However, their therapeutic potential is constrained by low circulating abundance, short half-life, limited endocrine action, or incomplete understanding of their receptors and downstream functions.

Our study identifies NLGN3 as a previously unrecognized skeletal muscle-derived factor that mediates the metabolic benefits of exercise. Notably, obesity markedly reduced NLGN3 mRNA expression in skeletal muscle and lowered circulating NLGN3 levels. The reduced serum NLGN3 in obese sedentary mice relative to lean controls suggests that obesity-associated metabolic stress may reduce circulating NLGN3. Obesity-associated factors, including chronic inflammation and insulin resistance, may suppress NLGN3 synthesis, promote degradation, or impair its secretion or shedding from skeletal muscle and other peripheral tissues.

Although exogenous NLGN3 administration strikingly reduced body weight and fat mass in obese mice, the associated metabolic parameters were modest but significant. This likely reflects the short treatment duration and limited dosing, suggesting that more robust effects on glucose homeostasis may require prolonged or higher dosing and/or synergy with other exercise-induced factors. Thus, NLGN3 contributes to metabolic improvement but is unlikely to be a sole regulator of systemic glucose homeostasis. A previous study showed that overexpression of NLGN transcripts, including NLGN3, in pancreatic β -cells enhances insulin secretion, whereas their knockdown suppresses it (47),

indicating indirect effects of NLGN3 on regulating glucose homeostasis.

Given the key role of the hypothalamic arcuate and paraventricular nuclei in energy and glucose homeostasis (48,49), it will be important to determine whether exercise influences neuron-derived NLGN3. Although NLGN3-NRXN3 signaling within paraventricular circuits regulates body weight and glucose metabolism independently of food intake (45,49), there is no evidence that circulating NLGN3 crosses the blood-brain barrier. Its large size (~110 kDa) and lack of known transport mechanisms make direct brain access unlikely, highlighting the need for neuron-specific NLGN3 silencing to delineate central versus peripheral contributions in exercise-induced metabolic regulation.

A growing number of reports have indicated that metabolic and inflammatory signaling are tightly interconnected, particularly in WAT, where chronic low-grade inflammation drives metabolic dysfunction (50,51). Exercise-induced myokines modulate both metabolic pathways and inflammatory responses, reinforcing the concept of skeletal muscle as an endocrine organ (4,52). WAT plays a central role in glucose and lipid metabolism (53); however, in obesity, it becomes dysfunctional due to macrophage-driven chronic inflammation (35–38), impaired lipogenesis-lipolysis balance, and reduced insulin sensitivity in adipocytes (53). Accordingly, we focused on adipocytes and macrophages as key cellular targets. CM from exercise-mimicking skeletal muscle cells enhanced insulin signaling and glucose uptake in adipocytes; however, strong signaling responses did not proportionally translate into glucose uptake, likely due to rate-limiting factors such as Glut-4 abundance, feedback inhibition, or pathway divergence toward growth or lipid metabolism. Interestingly, despite lower NLGN3 levels in CM-FSK, adipocytes incubated with CM-FSK still exhibited improved insulin sensitivity, indicating that FSK induces additional muscle-derived mediators. Thus, NLGN3 contributes to, but does not fully account for, the metabolic effects of exercise-mimicking conditions.

Proteomic analysis of CM from skeletal muscle cells exposed to exercise mimetics identified 31 secretory proteins commonly enriched across all treatments and absent in controls. These proteins were ranked by mean abundance as a descriptive prioritization strategy to identify consistently enriched candidates, acknowledging that absolute abundance does not necessarily reflect physiological importance, as low-abundance proteins may also exert potent biological effects. Emerging evidence places NLGN3 within the sheddome or secretome (54,55). Importantly, NLGN3 is known to undergo

tissue browning markers (UCP1, TMEM26, PRDM16, and CD137), lipolysis markers (ATGL, HSL, and PLIN), and proinflammatory (iNOS, IL-6, and IL-1 β), and anti-inflammatory (ARG1, YM1, and IL-13) markers in the VAT from the respective treatment groups ($n = 3$). *I*: Representative immunofluorescence images (left) and quantification of fluorescence intensity (right) for ASC1 (white adipocyte marker, green) and SHOX2 (beige/brown adipocyte marker, red) in the VAT sections of these treatment groups ($n = 4$). *J*: Western blot analysis showing the abundance of pIR β (Y1345), pAkt (S473), and Glut-4 protein levels in the VAT from the respective treatment groups ($n = 3$). Total IR β , Akt1/2/3, and β -actin served as loading controls. *K*: Schematic representation of a proposed model depicting skeletal muscle and adipose tissue cross talk in the involvement of exercise-induced myokine NLGN3 in improving adipose tissue functions and insulin sensitivity in obese insulin-resistant conditions. Data are mean \pm SD. * $P < 0.05$, ** $P < 0.01$, *** $P < 0.001$, **** $P < 0.0001$.

ADAM10-mediated ectodomain shedding (56), allowing it to act as an intercellular signaling molecule. Exercise training has been linked to increased expression and activity of ADAM10 (57), which could drive NLGN3 shedding. Interestingly, we found that exercise elevates circulating NLGN3 mainly through proteolytic shedding rather than classical secretion. In contrast, neuronal activity induces vesicular secretion of NLGN3, which activates proliferative phosphoinositide 3-kinase–mammalian target of rapamycin and ERK signaling pathways in glioma cells (55). These observations suggest that the source, mode of release, and physiological context of NLGN3 critically determine its downstream effects. However, the mechanisms governing NLGN3 synthesis and its secretion or shedding from skeletal muscle following exercise stimulation remain unclear and warrant further investigation.

Although exercise increased NLGN3 mRNA expression in both skeletal muscle and WAT, the induction was substantially greater in skeletal muscle (~15-fold vs. ~8.5-fold), indicating that skeletal muscle is a major source of circulating NLGN3 with potential endocrine effects on WAT. However, contributions from other tissues and possible autocrine actions within WAT cannot be excluded. NLGN3 appears to regulate energy balance by modulating key metabolic pathways in WAT, and like other exercise-induced mediators (58), it enhances glucose uptake, suppresses adipogenesis, promotes lipolysis, and induces adipose browning, underscoring its role in adipose homeostasis. NLGN3 also skewed macrophages toward an anti-inflammatory phenotype, akin to exercise-induced myokines (59), accentuating its dual role in regulating adipocyte and macrophage function.

The current study has certain limitations that should be considered. First, as this study relied primarily on mouse models and cell lines, future investigations in lean and obese human participants with or without T2D, including analyses of WAT from various depots and BAT, will be critical to evaluate translational relevance of NLGN3. Second, exercise mimetic treatments do not fully recapitulate muscle contraction or capture differences in exercise strength, intensity, and duration. Comparing our findings with in vitro electrical pulse stimulation and in vivo exercise paradigms across exercise modalities (swimming vs. treadmill) would further validate our observations. Third, the signaling cascades downstream of NLGN3-NRXN1/3 interactions in adipocytes and macrophages, particularly in clinical and translational settings, remain to be fully elucidated. Finally, skeletal muscle–specific deletion of NLGN3, along with macrophage- and adipocyte-specific ablation of NRXN1 and NRXN3, respectively, will be essential to establish their causal roles in metabolic regulation.

With growing recognition of exercise-induced myokines in regulating metabolism, the discovery of exercise-responsive mediator NLGN3 with metabolic and immunomodulatory functions paves new avenues for exercise mimetic therapies. Therefore, targeting the NLGN3-NRXN1/3 axis may represent

a promising strategy to combat obesity-associated insulin resistance.

Acknowledgments. The authors thank Prof. Masashi Muroi from Mutsashino University for p55-CIB-luc plasmid; Sandor Life Sciences Pvt. Ltd., for LC-MS/MS analysis; and the National Centre for Cell Science for L6 rat skeletal myoblast, C2C12 mouse skeletal myoblast, RAW264.7 mouse macrophage, and HEK293 human embryonic kidney cell lines. The plasmids pCAG-HA-NLGN3 WT (RRID: Addgene_59318) and pCAG-HA-NLGN3 R451C (RRID: Addgene_59319) were a gift from Dr. Peter Scheiffele (University of Basel). The authors also thank Dr. Manoj Sharma (Tezpur University) for oil red O imaging; Dr. Gurumayum Chourajit Sharma (Tezpur University) for M1/M2 polarization flow cytometric analysis; and Dr. Ambuj Srivastava (University of California, San Diego) for assisting in submission of raw MS/MS files to ProteomeXchange via the PRIDE database. The authors are thankful to the heads of the Department of Molecular Biology and Biotechnology, Tezpur University; Department of Biomedical Engineering, Indian Institute of Technology Ropar; and National Institute of Pharmaceutical Education and Research for extending the facilities required for this investigation. We also acknowledge the support of the JNU-PAIR network on Science for Sustainable Future (ANRF/PAIR/2025/000029/PAIR) and DST-FIST-II (SR/FST/LSI-692/2016) to the Department of Molecular Biology and Biotechnology, Tezpur University.

Funding. A.S. and S.M. expresses their gratitude to the Indian Council of Medical Research (ICMR), Government of India, for the research fellowship. A.V. acknowledges the Council of Scientific and Industrial Research–Human Resource Development Group (CSIR-HRDG), Government of India for his research fellowship. This work was supported by the Department of Biotechnology (DBT) through Unit of Excellence grant BT/554/NE/U-Excel/2014 (to S.D.) and Twinning grant BT/PR24700/NER/95/819/2017 (to S.D. and D.Pal.), ICMR ad hoc grant 5/4/8-8/Obs/SD/2022-NCD-II (to S.D.), Department of Health Research Young Scientist Fellowship grant R.12014/81/2020-HR (to A.S.), and DBT/Wellcome Trust India Alliance Intermediate Fellowship/Grant IAI/23/2/506994 and CSIR-ASPIRE grant 37WS(0057)/2023-24/EMR-II/ASPIRE (to D.Pal.).

Duality of Interest. No potential conflicts of interest relevant to this article were reported.

Author Contributions. A.S., D.Pal., S.M., A.V., S.S., P.R., S.R., A.K., K.T., D.Pal., and S.D. analyzed the data sets. A.S., D.Pal., S.M., A.V., S.S., and S.R. designed and performed the experiments. U.D., and P.R. performed the proteomic data analysis and reanalysis of transcriptomic Gene Expression Omnibus data set GSE108643, respectively. A.K., K.T., D.Pal., and S.D. contributed resources. D.Pal. and S.D. conceived the idea, planned and designed the experiments, supervised the study, and wrote the original draft of the manuscript. All authors edited and reviewed the manuscript. D.Pal. and S.D. are the guarantors of this work and, as such, had full access to all the data in the study and take responsibility for the integrity of the data and the accuracy of the data analysis.

References

- International Diabetes Federation. *IDF Diabetes Atlas*. 10th ed. Brussels, International Diabetes Federation, 2022
- Yashi K, Garg C, Daley SF. Obesity and type 2 diabetes. In: *StatPearls*. Treasure Island, FL, StatPearls Publishing, 2025. Available from <https://www.ncbi.nlm.nih.gov/books/NBK592412/>
- Pedersen BK, Febbraio MA. Muscle as an endocrine organ: focus on muscle-derived interleukin-6. *Physiol Rev* 2008;88:1379–1406
- Pedersen BK, Febbraio MA. Muscles, exercise and obesity: skeletal muscle as a secretory organ. *Nat Rev Endocrinol* 2012;8:457–465
- Schnyder S, Handschin C. Skeletal muscle as an endocrine organ: PGC-1 α , myokines and exercise. *Bone* 2015;80:115–125
- Egan B, Zierath JR. Exercise metabolism and the molecular regulation of skeletal muscle adaptation. *Cell Metab* 2013;17:162–184

7. Stanford KI, Goodyear LJ. Exercise and type 2 diabetes: molecular mechanisms regulating glucose uptake in skeletal muscle. *Adv Physiol Educ* 2014;38:308–314
8. Whitham M, Febbraio MA. The ever-expanding myokine: discovery challenges and therapeutic implications. *Nat Rev Drug Discov* 2016;15:719–729
9. Huh JY. The role of exercise-induced myokines in regulating metabolism. *Arch Pharm Res* 2018;41:14–29
10. Boström P, Wu J, Jedrychowski MP, et al. A PGC1- α -dependent myokine that drives brown-fat-like development of white fat and thermogenesis. *Nature* 2012;481:463–468
11. Kim KH, Jeong YT, Oh H, et al. Autophagy deficiency leads to protection from obesity and insulin resistance by inducing Fgf21 as a mitokine. *Nat Med* 2013;19:83–92
12. Rao RR, Long JZ, White JP, et al. Meteorin-like is a hormone that regulates immune-adipose interactions to increase beige fat thermogenesis. *Cell* 2014;157:1279–1291
13. Varoqueaux F, Aramuni G, Rawson RL, et al. Neuroligins determine synapse maturation and function. *Neuron* 2006;51:741–754
14. Tabuchi K, Blundell J, Etherton MR, et al. A neuroligin-3 mutation implicated in autism increases inhibitory synaptic transmission in mice. *Science* 2007;318:71–76
15. Ichtchenko K, Nguyen T, Südhof TC. Structures, alternative splicing, and neurexin binding of multiple neuroligins. *J Biol Chem* 1996;271:2676–2682
16. Tabuchi K, Südhof TC. Structure and evolution of neurexin genes: insight into the mechanism of alternative splicing. *Genomics* 2002;79:849–859
17. Harkin LF, Lindsay SJ, Xu Y, et al. Neurexins 1–3 each have a distinct pattern of expression in the early developing human cerebral cortex. *Cereb Cortex* 2017;27:216–232
18. Südhof TC. Neuroligins and neurexins link synaptic function to cognitive disease. *Nature* 2008;455:903–911
19. de Wit J, Ghosh A. Specification of synaptic connectivity by neuroligins and neurexins. *Nat Rev Neurosci* 2016;17:22–35
20. Reissner C, Runkel F, Missler M. Neurexins. *Genome Biol* 2013;14:213
21. Yu JH, Kim MS. Molecular mechanisms of appetite regulation. *Diabetes Metab J* 2012;36:391–398
22. Borgmeyer M, Coman C, Has C, et al. Multiomics of synaptic junctions reveals altered lipid metabolism and signaling following environmental enrichment. *Cell Rep* 2021;39:109797
23. Banerjee D, Patra D, Sinha A, et al. Lipid-induced monokine cyclophilin-A promotes adipose tissue dysfunction implementing insulin resistance and type 2 diabetes in zebrafish and mice models of obesity. *Cell Mol Life Sci* 2022;79:282
24. Choudhary SA, Patra D, Sinha A, et al. A small molecule potent IRAK4 inhibitor abrogates lipopolysaccharide-induced macrophage inflammation in-vitro and in-vivo. *Eur J Pharmacol* 2023;944:175593
25. Wang D, Zhang X, Li Y, et al. Exercise-induced browning of white adipose tissue and improving skeletal muscle insulin sensitivity in obese/non-obese growing mice: do not neglect exosomal miR-27a. *Front Nutr* 2022;9:940673
26. Parks BW, Sallam T, Mehrabian M, et al. Genetic architecture of insulin resistance in the mouse. *Cell Metab* 2015;21:334–347
27. Sun L, Luan J, Wang J, et al. GEPREP: a comprehensive data atlas of RNA-seq-based gene expression profiles of exercise responses. *J Sport Health Sci* 2025;14:100992
28. Choudhary SA, Bora N, Banerjee D, et al. A novel small molecule A2A adenosine receptor agonist, indirubin-3'-monoxide, alleviates lipid-induced inflammation and insulin resistance in 3T3-L1 adipocytes. *Biochem J* 2019;476:2371–2391
29. Banerjee D, Patra D, Sinha A, et al. Macrophage foam cell-derived mediator promotes spontaneous fat lipolysis in atherosclerosis models. *J Leukoc Biol* 2025;117:qiae210
30. Pal D, Dasgupta S, Kundu R, et al. Fetuin-A acts as an endogenous ligand of TLR4 to promote lipid-induced insulin resistance. *Nat Med* 2012;18:1279–1285
31. Patra D, Ramprasad P, Sharma S, et al. Adipose tissue macrophage-derived microRNA-210-3p disrupts systemic insulin sensitivity by silencing GLUT4 in obesity. *J Biol Chem* 2024;300:107328
32. Hardie DG. AMP-activated protein kinase: an energy sensor that regulates all aspects of cell function. *Genes Dev* 2011;25:1895–1908
33. Carter S, Solomon TPJ. In vitro experimental models for examining the skeletal muscle cell biology of exercise: the possibilities, challenges and future developments. *Pflugers Arch* 2019;471:413–429
34. Gubert C, Hannan AJ. Exercise mimetics: harnessing the therapeutic effects of physical activity. *Nat Rev Drug Discov* 2021;20:862–879
35. Shantaram D, Hoyd R, Blaszczak AM, et al. Obesity-associated microbiomes instigate visceral adipose tissue inflammation by recruitment of distinct neutrophils. *Nat Commun* 2024;15:5434
36. Weisberg SP, McCann D, Desai M, et al. Obesity is associated with macrophage accumulation in adipose tissue. *J Clin Invest* 2003;112:1796–1808
37. Lumeng CN, Bodzin JL, Saltiel AR. Obesity induces a phenotypic switch in adipose tissue macrophage polarization. *J Clin Invest* 2007;117:175–184
38. Saltiel AR, Olefsky JM. Inflammatory mechanisms linking obesity and metabolic disease. *J Clin Invest* 2017;127:1–4
39. Almagro Armenteros JJ, Tsigos KD, Sønderby CK, et al. SignalP 5.0 improves signal peptide predictions using deep neural networks. *Nat Biotechnol* 2019;37:420–423
40. Rutkowski JM, Stern JH, Scherer PE. The cell biology of fat expansion. *J Cell Biol* 2015;208:501–512
41. Roberts R, Hodson L, Dennis AL, et al. Markers of de novo lipogenesis in adipose tissue: associations with small adipocytes and insulin sensitivity in humans. *Diabetologia* 2009;52:882–890
42. Lafontan M, Langin D. Lipolysis and lipid mobilization in human adipose tissue. *Prog Lipid Res* 2009;48:275–297
43. Napetschnig J, Wu H. Molecular basis of NF- κ B signaling. *Annu Rev Biophys* 2013;42:443–468
44. Li T-L, Gleeson M. The effect of single and repeated bouts of prolonged cycling on leukocyte redistribution, neutrophil degranulation, IL-6, and plasma stress hormone responses. *Int J Sport Nutr Exerc Metab* 2004;14:501–516
45. Mu M, Sun H, Geng S, et al. Neurexin-3 in the paraventricular nucleus of the hypothalamus regulates body weight and glucose homeostasis independently of food intake. *Mol Brain* 2024;17:49
46. Steensberg A, van Hall G, Osada T, Sacchetti M, Saltin B, Klarlund Pedersen B. Production of interleukin-6 in contracting human skeletal muscles can account for the exercise-induced increase in plasma interleukin-6. *J Physiol* 2000;529(Pt. 1):237–242
47. Suckow AT, Comoletti D, Waldrop MA, et al. Expression of neurexin, neuroligin, and their cytoplasmic binding partners in the pancreatic beta-cells and the involvement of neuroligin in insulin secretion. *Endocrinology* 2008;149:6006–6017
48. Morton GJ, Meek TH, Schwartz MW. Neurobiology of food intake in health and disease. *Nat Rev Neurosci* 2014;15:367–378
49. Uchigashima M, Cheung A, Futai K. Neuroligin-3: a circuit-specific synapse organizer that shapes normal function and autism spectrum disorder-associated dysfunction. *Front Mol Neurosci* 2021;14:749164
50. Gregor MF, Hotamisligil GS. Inflammatory mechanisms in obesity. *Annu Rev Immunol* 2011;29:415–445
51. Wu H, Ballantyne CM. Metabolic inflammation and insulin resistance in obesity. *Circ Res* 2020;126:1549–1564
52. Severinsen MCK, Pedersen BK. Muscle-organ crosstalk: the emerging roles of myokines. *Endocr Rev* 2020;41:594–609
53. Morigny P, Boucher J, Arner P, Langin D. Lipid and glucose metabolism in white adipocytes: pathways, dysfunction and therapeutics. *Nat Rev Endocrinol* 2021;17:276–295
54. Martín-de-Saavedra MD, Santos MD, Penzes P. Intercellular signaling by ectodomain shedding at the synapse. *Trends Neurosci* 2022;45:483–498
55. Venkatesh HS, Johung TB, Caretti V, et al. Neuronal activity promotes glioma growth through neuroligin-3 secretion. *Cell* 2015;161:803–816

56. Bemben MA, Nguyen TA, Li Y, et al. Isoform-specific cleavage of neuroligin-3 reduces synapse strength. *Mol Psychiatry* 2019;24:145–160
57. Ennequin G, Boisseau N, Caillaud K, et al. Exercise training and return to a well-balanced diet activate the neuregulin 1/ErbB pathway in skeletal muscle of obese rats. *J Physiol* 2015;593:2665–2677
58. Barros D, Marques EA, Magalhães J, Carvalho J. Energy metabolism and frailty: The potential role of exercise-induced myokines - A narrative review. *Ageing Res Rev* 2022;82:101780
59. Zhou L, Long H, Alizadeh H. Meteorin-Like Protein (Metrl): An exercise-induced myokine with therapeutic potential in metabolic and inflammatory disorders. *Obes Rev* 2026;27:e70046